INTERNATIONAL JOURNAL FOR NUMERICAL METHODS IN FLUIDS
Int. J. Numer. Meth. Fluids 2009; **61**:1273–1298
Published online 20 January 2009 in Wiley InterScience (www.interscience.wiley.com). DOI: 10.1002/fld.1999

Computation of head–disk interface gap micro flowfields using DSMC and continuum–atomistic hybrid methods

Benzi John[‡] and M. Damodaran[*, †, §]

Division of Thermal and Fluids Engineering, School of Mechanical and Aerospace Engineering, Nanyang Technological University, 50 Nanyang Avenue, 639798 Singapore, Singapore

SUMMARY

This paper discusses computational modeling of micro flow in the head–disk interface (HDI) gap using the direct simulation Monte Carlo (DSMC) method. Modeling considerations are discussed in detail both for a stand-alone DSMC computation and for the case of a hybrid continuum–atomistic simulation that couples the Navier–Stokes (NS) equation to a DSMC solver. The impact of the number of particles and number of cells on the accuracy of a DSMC simulation of the HDI gap is investigated both for two- and three-dimensional configurations. An appropriate implicit boundary treatment method for modeling inflow and outflow boundaries is used in this work for a three-dimensional DSMC micro flow simulation. As the flow outside the slider is in the continuum regime, a hybrid continuum–atomistic method based on the Schwarz alternating method is used to couple the DSMC model in the slider bearing region to the flow outside the slider modeled by NS equation. Schwarz coupling is done in two dimensions by taking overlap regions along two directions and the Chapman–Enskog distribution is employed for imposing the boundary condition from the continuum region to the DSMC region. Converged hybrid flow solutions are obtained in about five iterations and the hybrid DSMC–NS solutions show good agreement with the exact solutions in the entire domain considered. An investigation on the impact of the size of the overlap region on the convergence behavior of the Schwarz method indicates that the hybrid coupling by the Schwarz method is weakly dependent on the size of the overlap region. However, the use of a finite overlap region will facilitate the exchange of boundary conditions as the hybrid solution has been found to diverge in the absence of an overlap region for coupling the two models. Copyright © 2009 John Wiley & Sons, Ltd.

Received 5 August 2008; Revised 21 October 2008; Accepted 3 December 2008

KEY WORDS: DSMC; continuum–atomistic hybrids; micro flow simulation; head–disk interface; slider bearing; Schwarz method

[*]Correspondence to: M. Damodaran, Division of Thermal and Fluids Engineering, School of Mechanical and Aerospace Engineering, Nanyang Technological University, 50 Nanyang Avenue, 639798 Singapore, Singapore.
[†]E-mail: mdamodaran@ntu.edu.sg
[‡]Graduate Research Student.
[§]Associate Professor.

Contract/grant sponsor: Seagate Technology International and Nanyang Technological University

1. INTRODUCTION

The direct simulation Monte Carlo (DSMC) method has been widely employed for modeling gaseous flows under rarefied flow conditions. Applications of the DSMC method range from simulation of hypersonic flow applications in the upper atmosphere such as reentry vehicles, orbital vehicles, etc to the simulation of low-speed gas flows in devices at micro and nano scales. In the case of upper atmosphere applications, rarefied gas flow conditions are caused by low-density conditions. The Knudsen number is typically used to find the degree of rarefaction involved, based on which different flow regimes could be identified. Under low-density conditions, the mean-free path is in the order of meters resulting in a high Knudsen number. MEMS applications typically operate under standard atmospheric (STP) conditions. The mean-free path of air at STP is in the order of nanometers and rarefied flow conditions in such applications are caused by the extremely small geometric dimensions involved which are of the order of micro/nano scales. Rarefied gas flow applications could also involve situations where both continuum and rarefaction regions occur simultaneously, thereby demanding the use of multi-scale methods.

A classic example of a rarefied flow at a nano scale is the flow that occurs in the head–disk interface (HDI) gap in a modern hard disk drive (HDD). As the HDI gap is of the order of a few nanometers, the flow in the gap will deviate from the continuum hypothesis and hence the modeling of this flow is best done using an appropriate flow model such as the DSMC method. The flow outside the HDI gap region is in the continuum regime and hence an appropriate multi-scale method is required to couple the continuum solutions to the DSMC solutions within the HDI region. The global airflow characteristics outside the HDI gap in the HDD enclosure have been previously investigated by various researchers [1–4] using conventional continuum flow models based on the incompressible Navier–Stokes (NS) equations. Previous applications of DSMC to compute flow within the HDI gap include those by Alexander *et al.* [5] and Huang *et al.* [6]. In this work, various flow modeling aspects for the DSMC method have been discussed in detail both for a stand-alone DSMC computation and for the case of a hybrid continuum–atomistic simulation, which is then applied to compute the flow near the vicinity of the HDI gap.

The DSMC method originally developed by Bird [7] is a physical model that is based on the discrete molecular nature of the system, essentially capturing the physics of a dilute gas governed by the Boltzmann equation. This method models the macroscopic behavior of a fluid based on the discrete molecular character of gases by simulating the motion, interaction and collision of representative particles within an array of computational cells. The state of the system is defined by the positions and velocities of representative particles, which represent a large collection of real gas molecules. Although DSMC is a reliable and accurate method, it is computationally intensive due to the extremely small time steps, typically in the order of Pico seconds and to the linear cell dimensions that are much smaller than the mean-free path involved in the flow computation. These constraints limit the size of the region that can be modeled by the DSMC under STP. Hence all the DSMC simulations reported in this work have been done using the parallel DSMC method that can accelerate the flow modeling process. It is also important from the point of view of computational efficiency, to impose guidelines regarding the minimum number of cells and the number of particles per cell required without compromising the accuracy, especially so for a three-dimensional flow simulation. In this work, the impact of number of particles and number of cells on the accuracy of a DSMC simulation has also been investigated both for the two- and three-dimensional cases.

DOI: 10.1002/fld

The other issue of the DSMC flow simulation that requires special attention is the imposition of inflow and outflow boundary conditions. This aspect is particularly challenging for the DSMC method as boundary conditions are imposed at the inflow and outflow boundaries by injecting particles into the system with a molecular velocity distribution corresponding to the mean flow macroscopic variables corresponding to the external flow. In this work, boundary condition treatments for the DSMC method have been discussed in detail both for a stand-alone DSMC computation and also for the case of a hybrid continuum–atomistic simulation. Various methods for treating the inflow/outflow boundary conditions for micro flows are discussed and an appropriate implicit boundary treatment method is used in this work for the three-dimensional DSMC micro flow simulation. Various multi-scale methods are also discussed in this work for coupling the DSMC model in the slider bearing region to the flow outside the slider modeled by NS equation. The majority of the multi-scale methods for flow modeling reported in the literature focus on the computation of hypersonic non-equilibrium flow applications. Application of multi-scale methods to low-speed gaseous flow applications in MEMS devices, however, has received due attention only recently and reported works are very limited in this area. In the current work, a multi-scale method based on the Schwarz alternating method, which is the appropriate method for incompressible flow applications, is employed for the hybrid coupling. The hybrid coupling is done by employing overlap regions along two directions (two-dimensional coupling) with the aid of the Chapman–Enskog velocity distribution function for boundary condition imposition from the continuum to the atomistic regime. By the Schwarz method, coupling is achieved by the iterative exchange of Dirichlet boundary conditions across an overlap region between the continuum and atomistic sub-domains. Various flow modeling aspects for this hybrid coupling are discussed in detail followed by the implementation of the Schwarz method. The impact of the size of the overlap region on the convergence behavior of the Schwarz method is also investigated.

2. DSMC SIMULATION METHOD

DSMC is a particle method based on the kinetic theory for the simulation of dilute gases. A detailed explanation of the steps involved in the DSMC method can be found in Bird [7]. The evolution of molecules is determined by tracking their positions and velocities. Starting from a set of initial conditions, the flow develops in a physically realistic manner by evaluating the collisions between the particles, boundary interactions of the particles with the wall and at the inflow/outflow boundaries. In contrast to the molecular dynamics method, the exact trajectory of each particle is not calculated in DSMC; instead a stochastic algorithm is used to evaluate the collision probabilities and scattering distributions based on kinetic theory. The time step in the DSMC simulation is much smaller than the mean-free time (mean time between successive collisions of particles), the collision between the particles can be decoupled from the positional changes of the particle for each time step, i.e. the particles are moved as if they do not interact and collision is considered only after all the particles have moved during the time step. The particles in the simulation are considered to be hard spheres. The particle–wall interactions are assumed to be inelastic and follow the diffuse reflection model with full thermal accommodation. The macroscopic properties such as the flow velocity, etc are derived as averages during the sampling phase once the system attains a steady state.

Figure 1 shows a schematic of a typical three-dimensional slider bearing geometry, which is representative of the HDI gap between the slider and the hard disk. The computational domain

DOI: 10.1002/fld

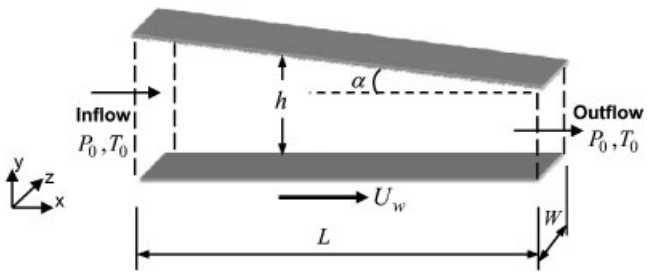

Figure 1. Schematic of three-dimensional slider geometry and computational domain.

is of length L and width W in which the flow is simulated using the DSMC method. The lower wall represents the spinning disk region moving with a tangential velocity U_w relative to the upper wall, which represents the slider surface. The channel height h varies along the length of the slider as the slider is inclined at a pitch angle α relative to the lower wall. The channel height at the inflow boundary is denoted by H_1, while that at the outflow boundary that represents the flying height is denoted by H_0. For the three-dimensional slider shown in Figure 1, the inflow boundary is represented by the y–z plane at the entrance, while all the other three sides of the slider are treated as outflows. At the inflow and outflow boundaries of the slider bearing, ambient conditions of pressure $P_0 = 1\,\text{atm}$ and temperature $T_0 = 273\,\text{K}$ are imposed by injecting particles with appropriate molecular velocity distribution from the inflow/outflow boundaries. The inflow and outflow boundary conditions for micro flows are discussed next.

2.1. *Considerations for imposing boundary conditions*

The inflow/outflow boundary conditions in a DSMC simulation are implemented by injecting particles into the system corresponding to the external flow conditions. The number of particles to be injected is derived from the density information, while the molecular velocity distribution of the injected particles must correspond to the mean flow macroscopic variables characteristic to the external flow as have been outlined in works such as that by Bird [7], Lilley and Macrossan [8] and Tysanner and Garcia [9]. For hybrid continuum–atomistic methods that couple the continuum solutions to the DSMC region, reservoir regions upstream and downstream of the inflow/outflow boundaries are incorporated to impose the boundary conditions. Particles must fill the reservoir region with a molecular velocity distribution corresponding to the flow velocity and velocity gradients in the continuum solutions. The equilibrium Maxwellian distribution function representation of the continuum equations is adequate for Euler equations, but in the case of the NS equations, the Chapman–Enskog distribution must be used as given in Chapman and Cowling [10].

For stand-alone DSMC computations, boundary conditions are often based on the equilibrium Maxwell–Boltzmann distribution function. In such cases particles are typically injected from the inflow/outflow boundary face, such that the velocity component of the injected particles u, which is normal to the inflow/outflow boundary corresponds to the biased Maxwellian distribution function. The other two molecular velocity components v and w are obtained separately from the ordinary Maxwellian distribution function. Besides the molecular velocity information, mean flow parameters such as density, temperature and velocity also need to be known to correctly set the properties of the incoming molecules at the inflow and the outflow boundaries. For high-speed

DOI: 10.1002/fld

compressible flow applications, given the density and the mean flow velocity of the external flow, the mean flow parameters of the injected particles can be directly set as corresponding to the free stream boundary condition. In micro flow applications, as the flow conditions near the inflow and outflow boundaries are not uniform owing to the influence from the presence of walls, free stream boundary conditions are not appropriate. Typically, in MEMS applications only the pressure information at the inflow and outflow boundaries is known *a priori*. Therefore, in such applications pressure boundary conditions are employed such that given the pressure information, other flow variables such as velocity are derived in an implicit manner as the flow simulation progresses to fix the boundary conditions.

2.2. *Pressure boundary conditions*

Various methods of implementing the implicit boundary treatment for the inflow and outflow boundaries for micro and nano scale flows modeled by the DSMC method have been proposed in the literature such as in Ikegawa and Kobayashi [11], Nance *et al.* [12] and Wu and Tseng [13]. One approach is the particle flux conservation concept in which the information on the number of particles crossing the boundaries is used to update the inflow velocity. The method of computing the inflow velocity at each time step using the particle flux conservation concept could result in errors under low-speed flow conditions, since the number of particles crossing the inflow boundary at low speed is very small and hence results in fluctuations in the imposed flow variables at the boundary. These fluctuations can be minimized by deriving the inflow velocity from the average number of particles entering the system over several time steps. Fang and Liou [14] had proposed a simple scheme by which a first-order extrapolation is used to determine the inflow mean velocity from the computed values at the cells inside the computational domain at the inflow boundary. However, the inflow velocity left uncorrected may not embody the pressure information and could be problematic if the wall temperature is different from the gas temperature. To overcome these difficulties, Wang and Li [15] had proposed a pressure correction scheme for both the inflow and outflow pressure boundaries based on the theory of characteristics and implemented the same for a two-dimensional simulation of poiseuille flow, orifice flow and corner flow in micro geometries. The advantage of the pressure boundary condition is that it does a feedback correction to fix the desired pressure conditions at the boundaries, by deriving the local mean flow parameters like the inflow and outflow velocity in an implicit manner as the simulation progresses. This approach has been extended in this work for the three-dimensional flow modeling in the slider bearing region.

The details of the treatment of boundary conditions at the inflow and outflow sections of the HDI gap at the entrance and exit given by the y–z plane as shown in Figure 1 are explained in this section. The number of particles, N, entering the computational domain from either the inflow or outflow boundary is determined from the Maxwellian distribution function

$$N = \Delta t\, An \frac{1}{2\beta\sqrt{\pi}} \{ e^{-\beta^2 U_j^2} + \beta\sqrt{\pi} U_j [1 + \mathrm{erf}(\beta U_j)] \} \tag{1}$$

where n is the number density at the inflow/outflow face, U_j represents the normal local mean flow velocity component at the boundary, A the cross-sectional area of the inflow/outflow face and $\beta = 1/\sqrt{2RT}$ where R is the universal gas constant.

The velocity component distribution of the injected particles is determined as follows. The velocity component, u, of the particles entering the computational domain, which is normal to the inflow or outflow boundary is generated using the acceptance–rejection procedure since it

DOI: 10.1002/fld

corresponds to the biased Maxwell–Boltzmann distribution. The molecular velocity components v and w parallel to the y and z axes of the y–z plane are obtained independently by sampling from the velocity distribution characteristic of the external flow as

$$v = (\sqrt{-\ln(R_f)}/\beta)\cos(2\pi R_f) + V_j \tag{2}$$

$$w = (\sqrt{-\ln(R_f)}/\beta)\sin(2\pi R_f) + W_j \tag{3}$$

where V_j, W_j represent the local mean flow velocity components in the y and z directions, j is the cell at the inflow or outflow boundary and R_f is a random fraction which ranges from 0 to 1.

The mean flow parameters are determined as follows. At the inflow boundary the known flow variables are pressure, p_{in}, and temperature, T_{in}. The number density, n_{in}, can be then obtained from the equation of state as

$$(n_{in}) = \frac{P_{in}}{kT_{in}} \tag{4}$$

where k is the Boltzmann constant.

The inflow velocity is then changed adaptively during the course of the flow simulation to enforce the pressure boundary conditions. The mean inflow velocity is obtained implicitly from the pressure information based on the theory of characteristics as follows:

$$(U_{in})_j = U_j + (p_{in} - p_j)/\rho_j a_j \tag{5}$$

where the subscript j denotes the cell at the boundary, ρ is the density of air and a is the local speed of sound. Similarly, at the subsonic outflow boundary the only known flow parameter is the exit pressure p_e. The other flow variables such as density and mean flow velocity are determined implicitly during the course of the flow simulation as follows:

$$(\rho_e)_j = \rho_j + (p_e - p_j)/(a_j)^2 \tag{6}$$

$$(U_e)_j = U_j + (p_j - p_e)/\rho_j a_j \tag{7}$$

3. HYBRID CONTINUUM–ATOMISTIC MODELING

Rarefied gas flow applications often involve both continuum and rarefaction regions and span a wide range of Knudsen numbers. The DSMC method can model the entire Knudsen number regime accurately, but is computationally expensive to model the entire domain. This motivates the use of multi-scale methods, which can couple DSMC that models the rarefied regions with continuum models in the rest of the region. Hadjiconstantinou [16] provides a review of the recent developments in the field of hybrid continuum–atomistic methods. The applicability of various coupling schemes to different flow problems has been studied in Wijesinghe and Hadjiconstantinou [17]. Explicit flux-based coupling method is appropriate for hypersonic flows for which the characteristic timescale is comparable to the DSMC time step. Multi-scale methods applied to hypersonic compressible flow problems reported in the literature include that by Garcia *et al.* [18], Hash and Hassan [19] and Wadsworth and Erwin [20]. More recently, hybrid methods have been applied for incompressible flow problems especially for modeling of microfluidics in MEMS applications.

DOI: 10.1002/fld

A hybrid continuum–atomistic method that relies on an explicit state-based coupling scheme at each time step for hypersonic non-equilibrium flow applications has been reported recently by Schwartzentruber and Boyd [21]. However for low-speed flows, as typically encountered in MEMS applications, there is a wide disparity between the timescales of atomistic and continuum models and implicit methods provide a framework for coupled solutions. As a result explicit flux-based coupling for incompressible flow problems might be computationally prohibitive especially if the continuum sub-domain is very large. Also flux-based coupling is not suitable for low-speed flows because of the high statistical noise of the flux variables when compared with the state variables such as velocity. Hence, the Schwarz alternating method provides an implicit framework for obtaining coupled solutions for such cases.

The Schwarz method, which was originally developed as a domain decomposition method as outlined in Quarteroni and Valli [22] for solving partial differential equations, has been extended for hybrid continuum–atomistic coupling and was first applied to liquid flows by Hadjiconstantinou [23] and later for dense fluids by Werder *et al.* [24]. Wijesinghe and Hadjiconstantinou [17] demonstrated the Schwarz hybrid coupling for a driven cavity test problem by employing overlap regions in both the x and y directions (two-dimensional coupling) and employed the Chapman–Enskog distribution. Real applications of the Schwarz alternating method to hybrid continuum–atomistic methods for gaseous flows in MEMS devices are a paucity in the literature. The Schwarz method has been applied recently by Aktas *et al.* [25] to predict the flow field in microfluidic filters. They had considered an overlap region in just one direction (one-dimensional coupling) for the hybrid coupling of the continuum and atomistic sub-domains and employed the Maxwellian distribution function. A flux-based coupling scheme has been employed previously for the coupling of continuum and DSMC solutions for the slider bearing problem by Memnonov [26]. Initial results of the hybrid coupling by the Schwarz alternating method for the slider bearing problem have been reported in Benzi and Damodaran [27]. In the present work, the Schwarz alternating method is employed for the hybrid coupling of continuum and atomistic sub-domains to compute flow in the vicinity of the HDI gap and the impact of overlap size on the convergence behavior of the Schwarz method is investigated in detail. By the Schwarz alternating method, the coupling between the continuum and atomistic sub-domains is attained implicitly by iterating between the steady-state solutions of the two sub-domains. An overlap region between the NS and atomistic regions facilitates the information exchange between the two domains in the form of Dirichlet boundary conditions. Exchange of flow variables such as velocity components when compared with the exchange of flux variables ensures that the statistical errors associated with DSMC can be minimized [28]. Schwarz iterations are done with updated boundary conditions in each sub-domain until solutions of both sub-domains are identical in the overlap region. From the point of view of computational efficiency, the atomistic region modeled by the DSMC method must be confined to rarefied regions while the remaining larger domain must be modeled as part of the continuum regime. One-dimensional Schwarz coupling employed by considering overlap region along one direction implies that the region modeled by DSMC for each Schwarz iteration could be very large resulting in poor computational efficiency. Thus for an optimum computational efficiency a two-dimensional coupling must be employed by considering overlap regions along both the x and y directions. In this work, the application of Schwarz coupling is demonstrated in two dimensions using the Chapman–Enskog distribution for boundary condition imposition from the continuum region to the DSMC region. The schematic of the two-dimensional geometry with the decomposition of the simulation domain into NS and DSMC sub-domains is shown in Figure 2. In the continuum domain, the incompressible NS equation is solved using the commercial flow solver

DOI: 10.1002/fld

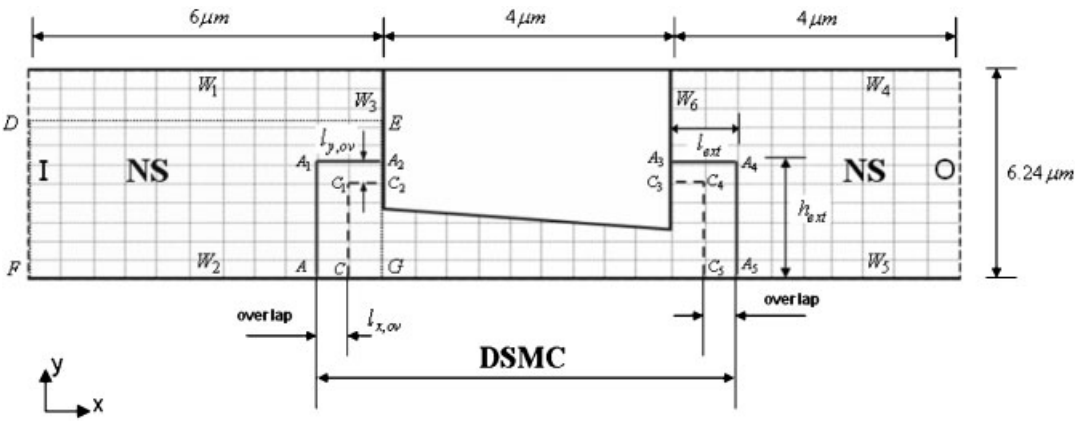

Figure 2. Schematic of two-dimensional computational domain showing DSMC and NS sub-domains with overlap region.

Fluent [29] which uses the finite volume method with the pressure equation derived using the SIMPLE method. The region under the slider and additional regions near the inflow and outflow is considered as the atomistic region that is modeled by DSMC, whereas the rest of the region is considered as the continuum domain modeled by the NS equations. The slider bearing region considered is of length $L=4\,\mu$m, flying height $H_0=25$ nm, pitch angle $\alpha=0.01$ rad and the bottom wall velocity $U_w=50$ m/s. Additional regions of length $l_{ext}=1.5\,\mu$m and height $h_{ext}=156$ nm at either side of the slider are also considered as part of the DSMC sub-domain as shown.

In Figure 2, the solid lines AA_1A_2 and $A_3A_4A_5$ represent the atomistic boundary that receives the flow variables from the continuum domain, whereas the dotted lines CC_1C_2 and $C_3C_4C_5$ represent the continuum sub-domain boundary that receives flow variables from the atomistic sub-domain. Schwarz coupling is done in two dimensions, for which overlap regions are considered both along the x and y directions as shown. The overlap along the x direction will be referred to as *x-overlap* which is of width $l_{x,ov}$, whereas the overlap along the y direction will be referred to as *y-overlap* which is of width $l_{y,ov}$. A similar overlap width is considered at both the inflow and outflow section with $l_{x,ov}=0.5\,\mu$m and $l_{y,ov}=39$ nm. A small selected region upstream of the slider denoted by the dotted rectangular region *DEFG* as shown in Figure 2 is chosen to make contour plots of the hybrid solution obtained. In the NS sub-domain the flow conditions are considered as incompressible and isothermal. The no-slip boundary condition is applied at all the walls denoted by W_{1-6} in the NS sub-domain as shown. The inlet boundary of the computational domain denoted by I in the figure is treated as a *Pressure Inlet*, whereas the outlet boundary denoted by O is specified as *Pressure Outlet* by which ambient pressure condition of $P_0=1$ atm is specified.

Figure 3 illustrates the boundary condition transfer for the hybrid coupling using the Schwarz alternating method. The DSMC and continuum sub-domains are tessellated using uniformly spaced rectangular cells. Dotted rectangular lines represent the cells in the continuum sub-domain and solid rectangular cells represent the DSMC cells. The macroscopic flow velocities (U_{DSMC}, V_{DSMC}) computed in the DSMC cells can be imposed directly as Dirichlet boundary conditions at the face centers of the continuum domain boundary Γ_{NS}. The macroscopic velocities are obtained by time

DOI: 10.1002/fld

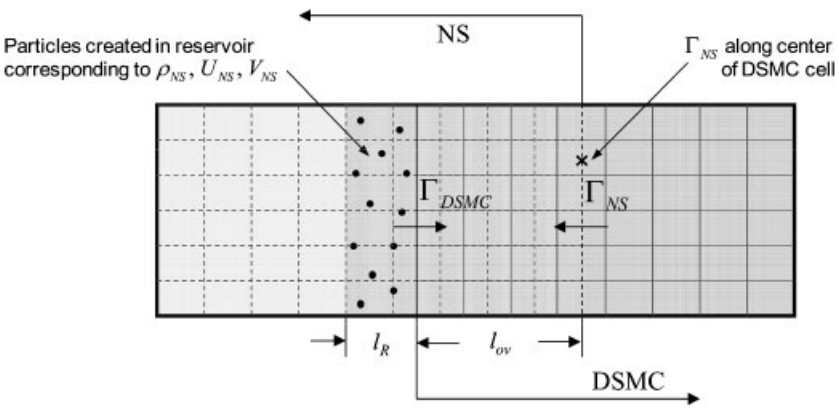

Figure 3. Schematic illustration of the Schwarz coupling method.

averaging the molecular velocities as normally done during the sampling phase in any standard DSMC procedure as follows:

$$U_{\mathrm{DSMC}} = \frac{1}{N_{\mathrm{c}}} \sum_{i=1}^{N_{\mathrm{c}}} u_i \tag{8}$$

$$V_{\mathrm{DSMC}} = \frac{1}{N_{\mathrm{c}}} \sum_{i=1}^{N_{\mathrm{c}}} v_i \tag{9}$$

where N_{c} is the number of particles in the cell, (u_i, v_i) are the molecular velocity components. The computed flow velocity field from the DSMC cells is extracted and used in the continuum domain (in which NS equations are solved using *Fluent*) as a boundary profile or via a user-defined function in *Fluent*. In order to mitigate the interpolation errors at the continuum boundary, the rectangular cells used for both the DSMC and continuum domains are taken to be of equal size and the face centers of the continuum cells along the boundary Γ_{NS} are aligned with the centers of the DSMC cells as shown in Figure 3.

The boundary conditions from the continuum sub-domain to the DSMC sub-domain are imposed using buffer cells (located adjacent to the boundary of the DSMC sub-domain Γ_{DSMC}) that act as a volume reservoirs filled with particles according to the density and velocity distribution corresponding to the NS solution in the continuum cells. The number of particles generated corresponds to the density information ρ_{NS} in the continuum cells. The Chapman–Enskog molecular velocity distribution is used to generate particles corresponding to the flow velocity $(U_{\mathrm{NS}}, V_{\mathrm{NS}})$ and velocity gradients in the NS sub-domain. The reservoir region is of length l_{R} as shown in Figure 3 and l_{R} is assumed such that it is sufficient to represent the entire range of velocity distribution function including the portion of the distribution function corresponding to the high-velocity fraction. The length of the reservoir region for the Chapman–Enskog distribution is the same as that for the Maxwellian distribution function. In the presence of a mean flow velocity U, the length of the reservoir region is taken as $l_{\mathrm{R}} = v_{\mathrm{cutoff}} \times \mathrm{d}t$ where $v_{\mathrm{cutoff}} = 6 \times (V_{\mathrm{mp}} + U)$ is the cutoff velocity, V_{mp} is the most probable velocity and $\mathrm{d}t$ is the time step. This ensures that the length of the reservoir is adequate enough to represent the entire range of Chapman–Enskog velocity distributions. The Chapman–Enskog distribution can be generated numerically by the

DOI: 10.1002/fld

acceptance–rejection method as outlined in Garcia and Alder [30]. The Chapman–Enskog velocity distribution $f(C)$ is given as follows:

$$f(C) = f_0(C)\Gamma(C) \tag{10}$$

where $f_0(C)$ is the Maxwellian distribution and C is the normalized thermal velocity whose components (C_x, C_y, C_z) are given by

$$C_x = (u - U_{\mathrm{NS}})/V_{\mathrm{mp}}, \quad C_y = (v - V_{\mathrm{NS}})/V_{\mathrm{mp}}, \quad C_z = (w)/V_{\mathrm{mp}} \tag{11}$$

where (u, v, w) represents the molecular velocity components and V_{mp} is the most probable velocity given by $V_{\mathrm{mp}} = (2kT/m)^{1/2}$

$$f_0(C) = \frac{1}{\pi^{3/2}} \mathrm{e}^{-C^2} \tag{12}$$

$\Gamma(C)$ is given by

$$\Gamma(C) = 1 + (q_x C_x + q_y C_y + q_z C_z)(\tfrac{2}{5}C^2 - 1) - 2(\tau_{xy} C_x C_y + \tau_{xz} C_x C_z + \tau_{yz} C_y C_z) - \tau_{xx}(C_x^2 - C_z^2) - \tau_{yy}(C_y^2 - C_z^2) \tag{13}$$

$$q_i = -\frac{k}{P}\left(\frac{2m}{kT}\right)^{1/2}\left(\frac{\partial T}{\partial x_i}\right) \tag{14}$$

$$\tau_{ij} = \frac{\mu}{P}\left(\frac{\partial v_i}{\partial x_j} + \frac{\partial v_j}{\partial x_i} - \frac{2}{3}\frac{\partial v_k}{\partial x_k}\delta_{i,j}\right) \tag{15}$$

where q_i and τ_{ij} are the dimensionless heat flux and stress tensor, μ is the dynamic viscosity of air, k is the thermal conductivity, P is the pressure and $v = (U_{\mathrm{NS}}, V_{\mathrm{NS}})$ is the mean velocity. To implement the Chapman–Enskog distribution function numerically by acceptance–rejection theorem, the velocity components $(U_{\mathrm{NS}}, V_{\mathrm{NS}})$ and the velocity gradients $\partial U_{\mathrm{NS}}/\partial x$, $\partial U_{\mathrm{NS}}/\partial y$, $\partial V_{\mathrm{NS}}/\partial x$ and $\partial V_{\mathrm{NS}}/\partial y$ from the continuum domain are used to compute the values for $\Gamma(C)$. The cell-centered values of the velocity and their gradients across any required section are obtained using *Fluent*. At each time step the reservoir is filled with particles and convected. Those particles that enter the simulation domain are retained, while the rest are discarded. To reduce the computational time associated with the DSMC method, the DSMC code solving the atomistic regime has been parallelized. Eight processors have been deployed for the computation and to ensure a reasonable

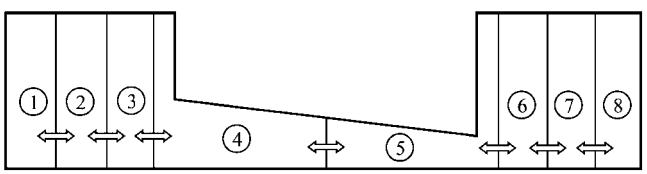

Figure 4. Schematic representation of partitioning of the DSMC sub-domain among eight processors for parallel processing.

DOI: 10.1002/fld

load balance among the processors, the partitioning of the computational domain is done such that each processor has approximately the same number of cells. The partitioning of the DSMC computational domain between processors to enable parallel computation is shown in Figure 4.

4. RESULTS AND DISCUSSION

For all the DSMC flow calculations considered in this work, the gaseous medium air is assumed to consist of monatomic molecules, each with a mass $m=6.63\times10^{-26}$ kg, diameter $d=3.66\times10^{-10}$ m and density $\rho=1.78\,\mathrm{kg/m^3}$. The time step for all the DSMC simulations is much smaller than the mean collision time and is five times smaller than $\Delta x/V_{\mathrm{mp}}$, where Δx is the smallest cell dimension and V_{mp} is the most probable molecular velocity. The parallel DSMC method outlined in Benzi and Damodaran [31] has been used to reduce the computational time.

4.1. DSMC slider bearing results

The impact of various parameters such as the number of cells and number of particles per cell on the accuracy of a DSMC simulation for the slider bearing application is considered in this section. The general guideline for an accurate DSMC simulation is that cell dimensions must be less than a mean-free path long and the time step less than the mean collision time with an average of at least 20–25 particles per cell. However, these constraints are problem specific and could be relaxed depending on the flow velocity and gradients of the specific problem under consideration. As DSMC is computationally intensive, it is important to have guidelines regarding the minimum number of cells and number of particles per cell required without compromising the accuracy, especially for a three-dimensional simulation and hence this investigation is done for the slider bearing application. On the basis of this study, adequate care has been taken to ensure the accuracy of the DSMC simulations for the HDI gap.

4.1.1. Two-dimensional DSMC flow simulations. The effect of the number of simulated particles per cell on the accuracy of the DSMC solutions for a two-dimensional simulation is investigated. The investigation has been done for a slider configuration shown in Figure 1 with $L=4\,\mu$m, flying height $H_0=25$ nm and a tangential velocity $U_{\mathrm{w}}=25$ m/s. Five DSMC simulations using an average of about 10, 20, 25, 35 and 50 particles per cell have been carried out. Figure 5 shows the effect of the number of particles per cell on the accuracy of the solutions of pressure and flow velocity distribution along the extent of the slider length on the lower wall or disk surface. It can be observed that for all the cases using 20 or more particles per cell the variation between the computed flow solutions is not significant, besides some statistical fluctuations. The convergence rate for the different cases considered is shown in Figure 6 by plotting the absolute average error with respect to the case with the largest number of particles per cell considered. For example, the absolute average error for pressure is calculated as $|P_{\mathrm{ref,av}}-P_{\mathrm{av}}|/P_{\mathrm{ref,av}}$, where P_{av} is the average value of pressure over the entire section and $P_{\mathrm{ref,av}}$ is the average value for the case with 50 particles per cell. It seems that the accuracy of the solutions has not improved further for cases using more than 20 particles per cell implying that 20 particles or more per cell are adequate enough for an accurate DSMC simulation in the HDI gap.

DOI: 10.1002/fld

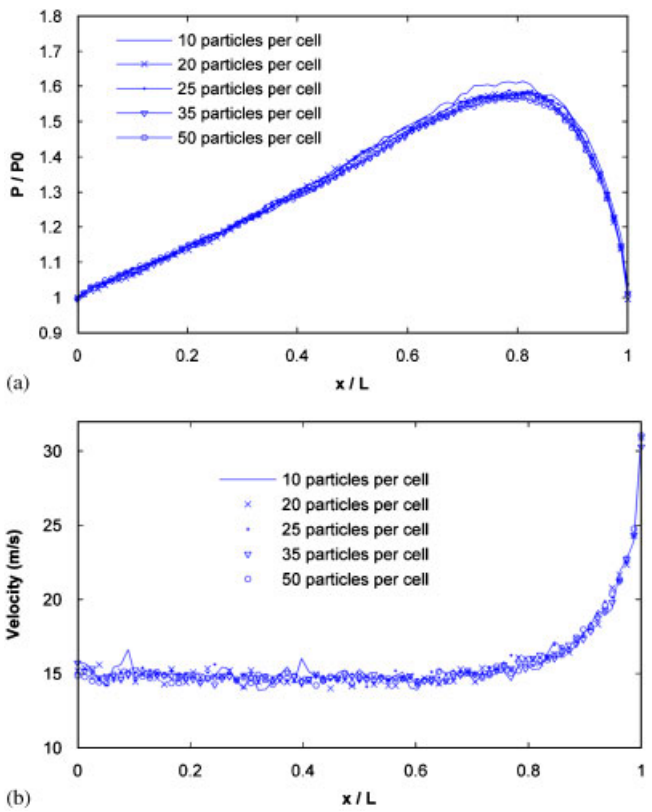

Figure 5. Effect of the number of particles on the accuracy of: (a) pressure and (b) velocity variation along the extent of the slider lower wall (or disk surface).

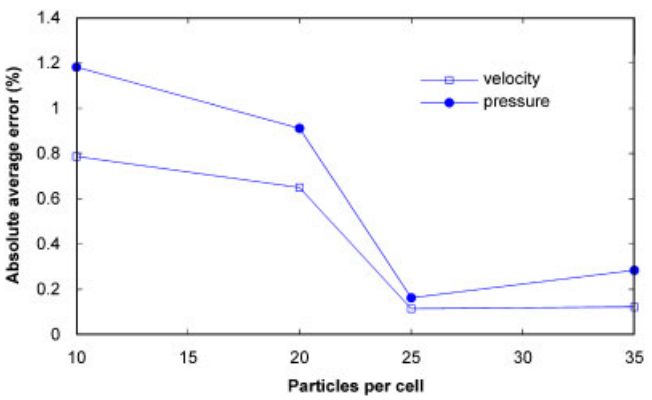

Figure 6. Average absolute error for pressure and velocity versus number of particles per cell.

DOI: 10.1002/fld

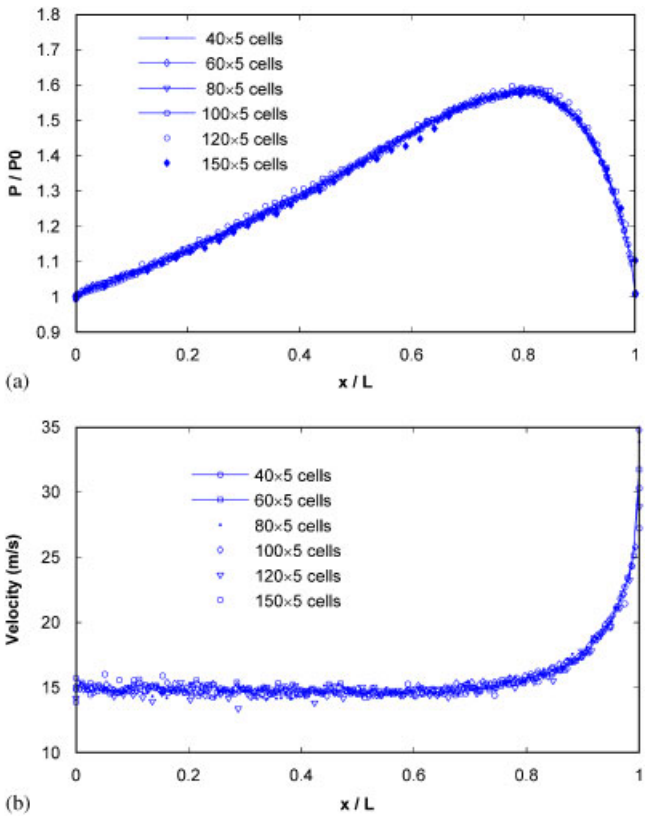

Figure 7. Effect of the number of cells on the accuracy of computed: (a) pressure and (b) velocity distribution along the extent of the slider lower wall (or disk surface).

The effect of the number of cells on the computed flow field is assessed by using 40×5, 60×5, 80×5, 100×5, 120×5 and 150×5 cells, which corresponds, respectively, to cell dimensions of about $1.6, 1.07, 0.8, 0.64, 0.53$ and 0.43 times the mean-free path in the flow direction. All the cases considered are based on an average of about 35 particles per cell. Figure 7 shows the effect of cell size on the variation of the computed pressure profile and flow velocity distribution along the bottom wall. The convergence rate with increase in number of cells is shown in Figure 8 by plotting the absolute average error with respect to the case with the largest number of cells considered, i.e. 150×5 cells. It is seen that by increasing the total number of cells along the flow direction, the error in the computed flow solutions is negligible and the accuracy of the solution is not improved further. This suggests that since the velocity gradients in the flow direction are negligible for the case of a slider bearing, cell dimensions in the flow direction can be even greater than a mean-free path.

4.1.2. Three-dimensional DSMC flow simulations. The impact of the number of particles per cell has also been investigated for a three-dimensional slider bearing configuration shown in Figure 1

DOI: 10.1002/fld

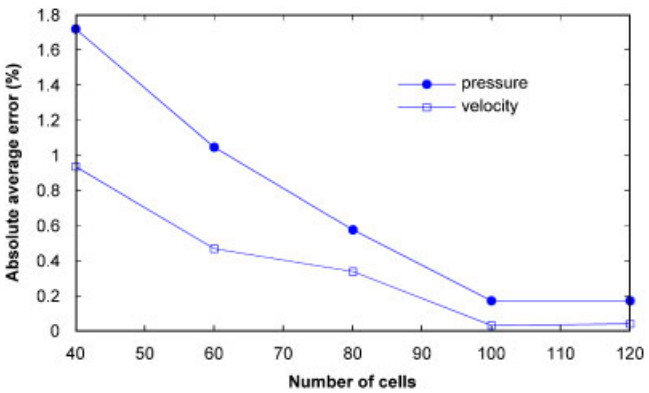

Figure 8. Average absolute error for pressure and velocity versus number of cells in the flow direction.

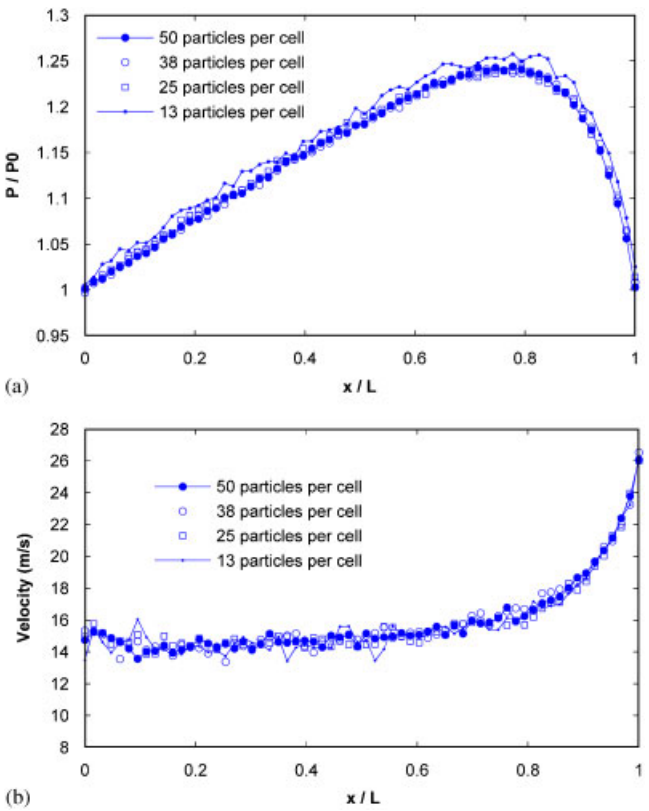

Figure 9. Effect of the number of particles on accuracy of: (a) pressure and (b) velocity solutions for three-dimensional DSMC along the disk surface.

DOI: 10.1002/fld

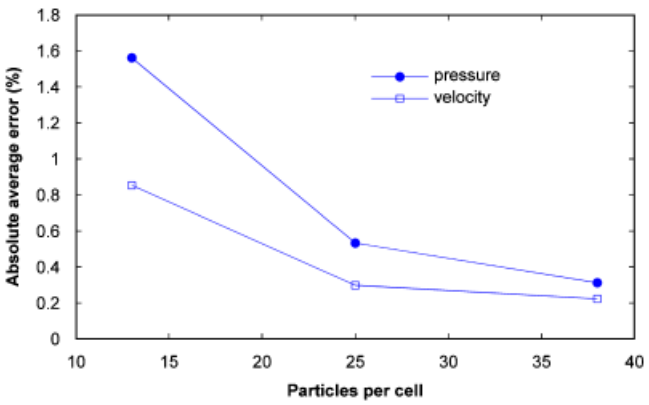

Figure 10. Average absolute error for pressure and velocity versus number of particles per cell.

with $L=3\,\mu$m, $W=3.3\,\mu$m, $H_0=25$ nm and $U_w=25$ m/s using the parallel DSMC code [31] for different number of particles viz. an average of about 13, 25, 38 and 50 particles per cell. The effect of the number of particles on the computed pressure and flow velocity distribution across a section along the disk surface located at $z/W=0.5$ is shown in Figure 9. The convergence rate with increase in number of particles per cell is shown in Figure 10 by plotting the absolute average error with respect to the case with 50 particles per cell. It can be seen that for the case corresponding to 25 particles per cell, the solution converges and further increase in the number of particles per cell seems to reduce the statistical fluctuations further. Based on this study, an average of about 30 particles per cell is used for all three-dimensional DSMC flow simulations considered in this work.

The effect of the number of cells in the z direction on the accuracy of a three-dimensional DSMC flow simulation is also investigated for varying cell sizes, viz. $64\times4\times20$, $64\times4\times30$, $64\times4\times40$, $64\times4\times50$ and $64\times4\times60$ cells, which corresponds to a cell dimension of about 2.64, 1.76, 1.32, 1.06 and 0.88 times the mean-free path in the z direction, respectively. Figure 11 shows the variation of the computed pressure profile along the disk surface corresponding to the various cell sizes. The corresponding absolute average error plot is also shown. It can be seen that increasing the number of cells in the z direction does not result in any observable increase in the accuracy. This suggests that cell dimensions can be much greater than the mean-free path in the z direction for a DSMC simulation in the HDI gap, where the velocity gradients are very small.

The variation of speedup (a performance metric defined as $S=T_s/T_p$, where T_s and T_p are the times taken for serial and parallel simulation, respectively) in the parallel three-dimensional parallel DSMC code with increase in number of particles per cell is shown in Figure 12. The performance analysis is done on *AlphaServer Supercomputer* (*SC45*), which is a distributed memory platform consisting of 44 nodes each having four 1 GHz processors with 1 GB memory and 8 MB cache. The performance curves show good scaling characteristics with super-linear speedups obtained for all the three cases considered, i.e. 20, 40 and 80 particles per cell. The super-linear speedup can be attributed to cache effects. By using multiple processors the size of sub-problem is reduced such that the data easily fit into caches resulting in significant reduction in memory access time. For a fixed load the parallel program scales up well up to a higher number of processors and with increase in number of particles per cell, significant improvement in performance is obtained.

DOI: 10.1002/fld

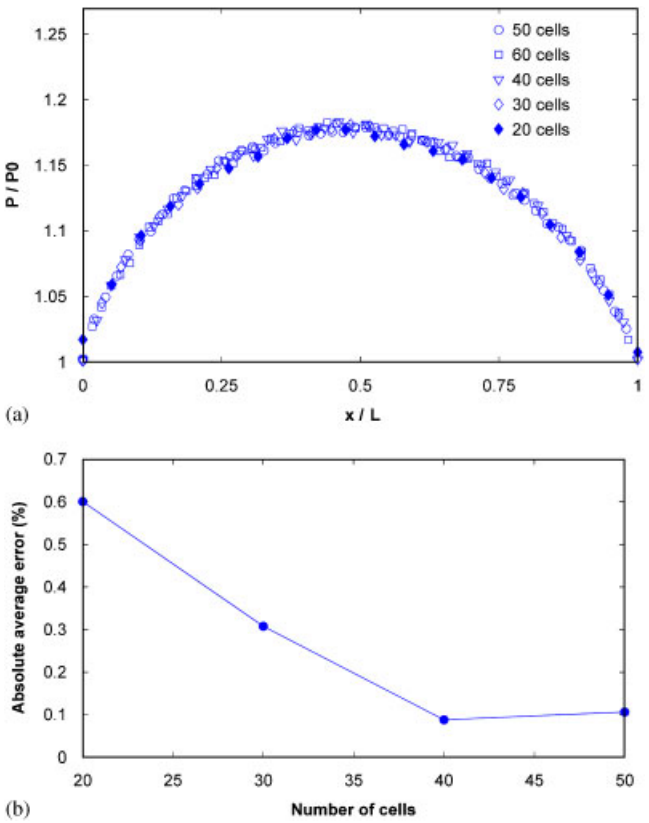

Figure 11. Plots of: (a) pressure profile along the disk surface and (b) absolute average error versus number of cells taken along the z direction.

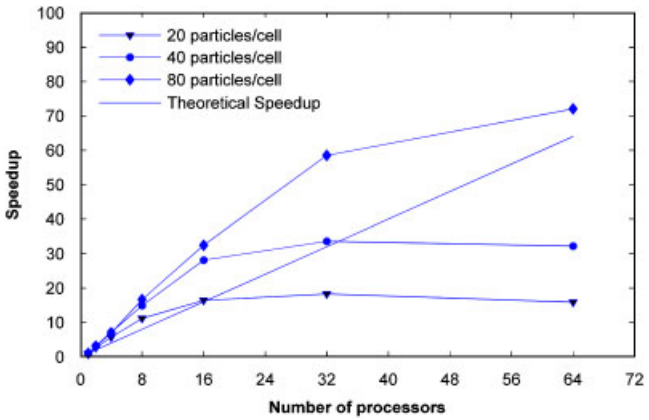

Figure 12. Speedup metric of the parallel DSMC code.

DOI: 10.1002/fld

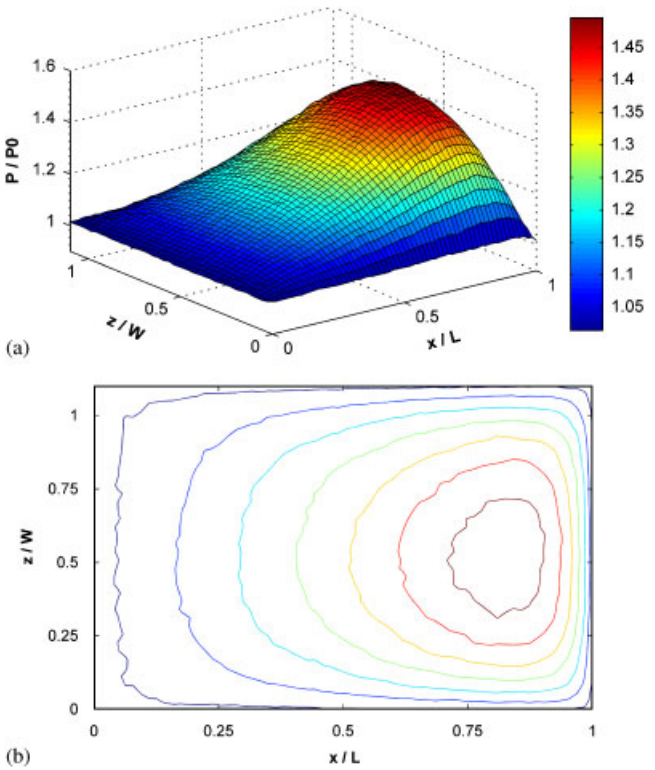

Figure 13. Computed pressure fields in the head–disk interface gap: (a) three-dimensional pressure profile and (b) pressure contours on the disk surface.

The computed pressure field in the three-dimensional slider bearing geometry for which $L=3\,\mu\text{m}$, $W=3.3\,\mu\text{m}$, $H_0=15\,\text{nm}$ and $U_w=25\,\text{m/s}$ is shown in Figure 13.

4.2. Hybrid continuum–atomistic flow solutions using Schwarz coupling

The Schwarz alternating method is applied to compute hybrid continuum–atomistic solutions in the vicinity of the HDI gap shown in Figure 2. The effect of grid size on the accuracy of the NS flow solutions in the continuum sub-domain has also been addressed. The grid convergence study has been conducted for the continuum sub-domain upstream of the slider with three different grid densities considered, i.e. 56 840, 85 200 and 113 680 cells. Figure 14 shows the variation of flow velocity in the y direction along a line taken at the mid section of the selected plane *DEFG* (shown in Figure 2) for the different grid cases. It can be seen from the plot that the flow solution does not change significantly with increase in grid density and hence adequate for an accurate flow simulation. For the NS simulations undertaken in this work the case with the finest grid density (i.e. 113 680 cells) is considered.

For the first Schwarz iteration, the DSMC sub-domain is solved using an initial guess boundary condition of $P=1\,\text{atm}$, $U_{NS}=0\,\text{m/s}$, $V_{NS}=0\,\text{m/s}$ at all the DSMC inflow and outflow boundaries. Additional Schwarz iterations are done using updated boundary conditions for each iteration

DOI: 10.1002/fld

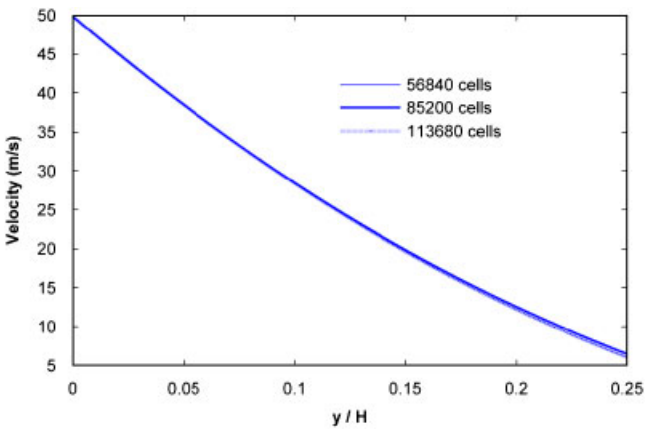

Figure 14. Plot of grid convergence showing variation of flow velocity with grid size in the NS domain.

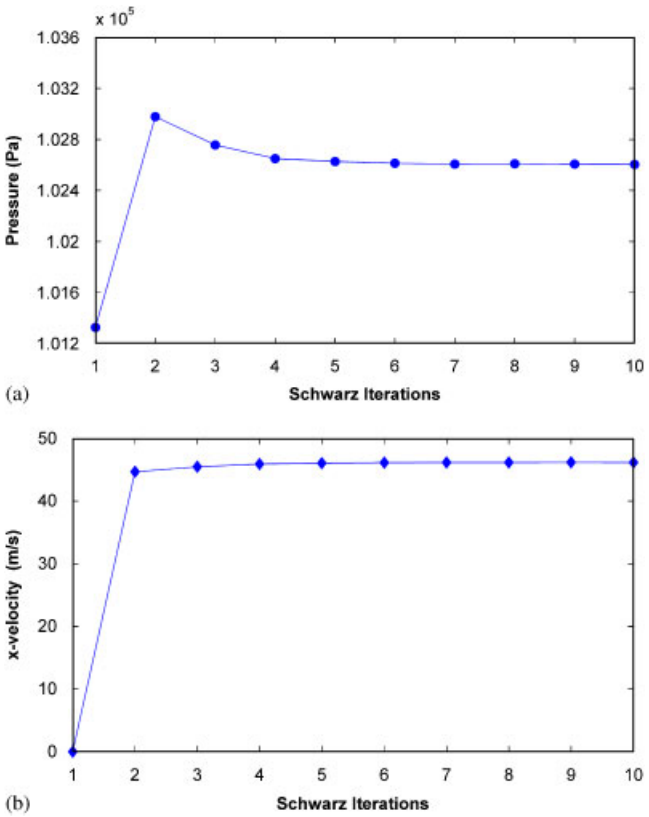

Figure 15. Convergence of: (a) pressure and (b) velocity boundary conditions transferred from continuum to DSMC along *x-overlap*.

DOI: 10.1002/fld

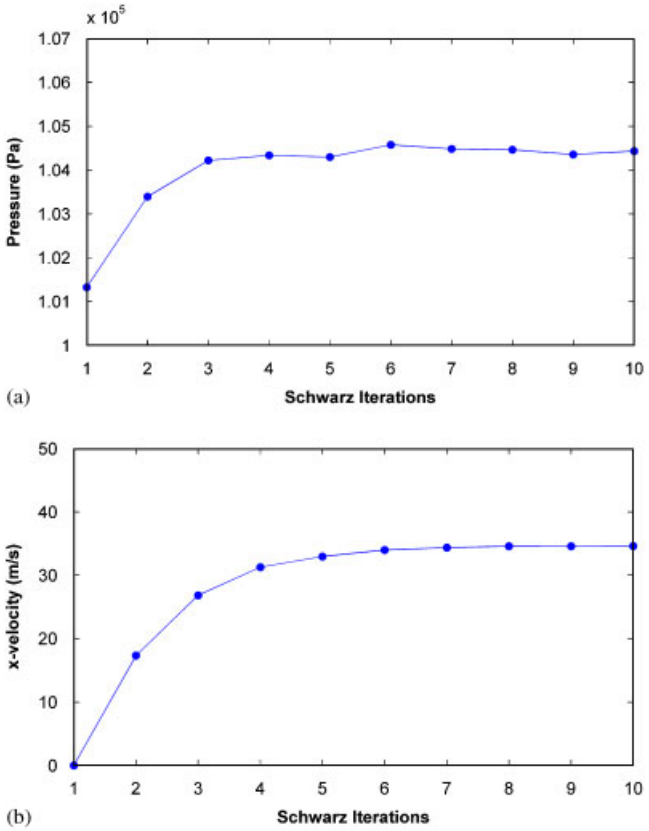

Figure 16. Convergence of: (a) pressure and (b) velocity boundary conditions transferred from continuum to DSMC along *y-overlap*.

until the solutions converge in the overlap region. The convergence of the Schwarz method can be assessed from the variation of velocity and pressure boundary conditions transferred from the continuum domain to the DSMC sub-domain with Schwarz iterations. The variation of the transferred velocity and pressure boundary conditions with Schwarz iteration along the *x-overlap* and *y-overlap* is shown in Figures 15 and 16. The boundary condition value along the *x-overlap* is plotted by taking the corresponding value from the buffer cell at $h_{\text{ext}}/2$, whereas the boundary condition value along the *y*-overlap is plotted by taking the corresponding value from the buffer cell at $l_{\text{ext}}/2$. It can be observed from the figures that convergence is attained in about five iterations after which the variations in the transferred boundary conditions are negligible.

Figure 17 shows the variation of the computed velocity components and pressure fields in the DSMC sub-domain with Schwarz iterations along a straight line located at a height of $0.15H_1$ above the bottom wall, where H_1 is the slider height at the leading edge. In the figure the region between the two vertical lines denotes the slider bearing region. It can be seen that the converged

DOI: 10.1002/fld

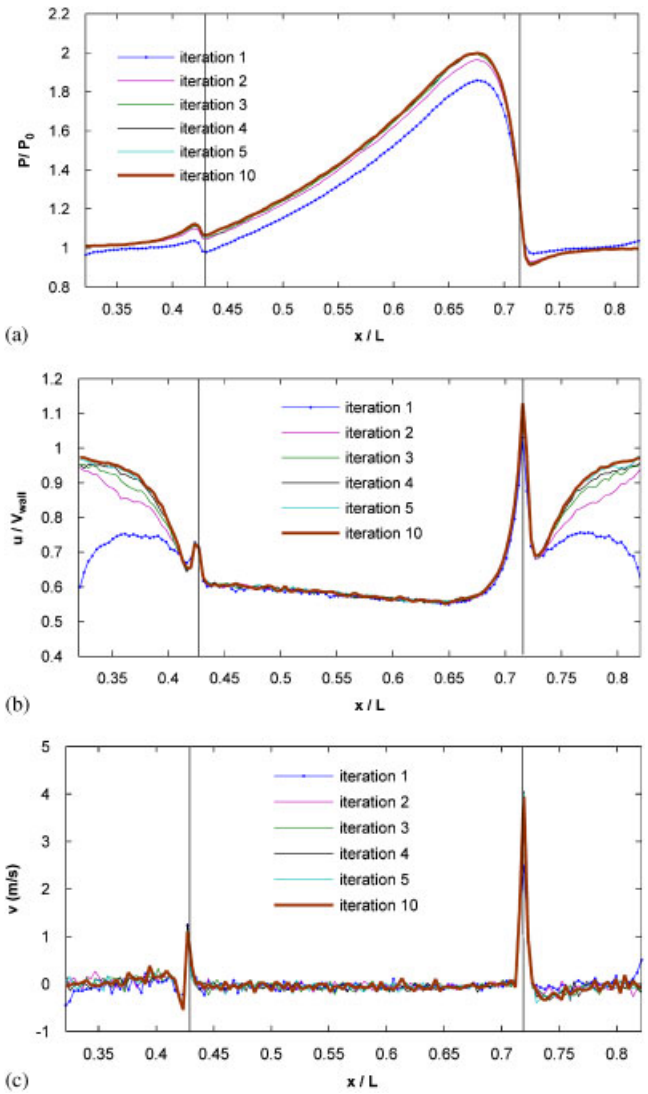

Figure 17. Variation of flow solutions of: (a) pressure; (b) *x-velocity*; and (c) *y-velocity* in the DSMC sub-domain with Schwarz iterations.

solutions for both pressure and velocity are obtained in about five iterations after which the solutions remain unchanged.

The computed velocity contour from the hybrid solutions obtained by combining the solutions in the continuum and atomistic regions across the selected plane *DEFG* (shown in Figure 2) located upstream of the slider is shown in Figure 18. The region between the dotted lines in the figure represents the overlap region.

DOI: 10.1002/fld

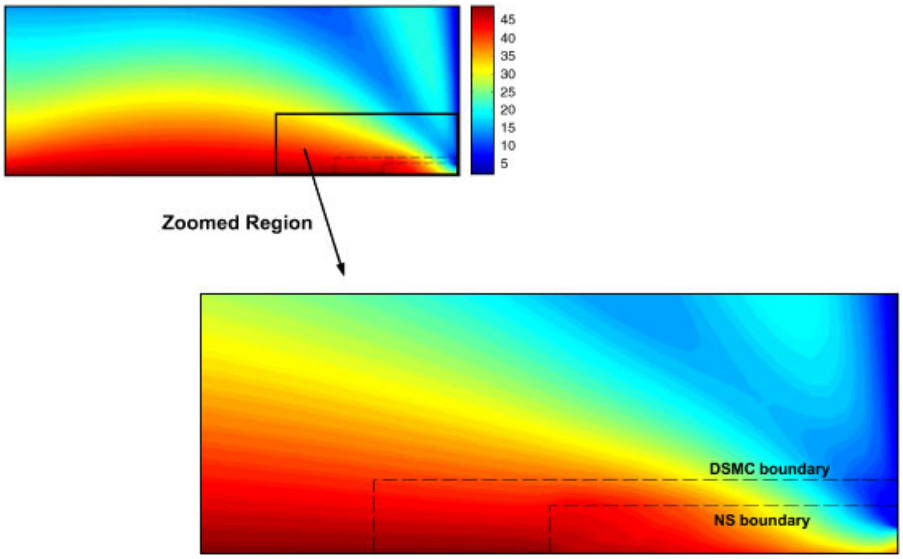

Figure 18. Velocity contour from the hybrid solution across a selected region upstream of the slider. (The region between the dotted lines represents the overlap region).

Figure 19 compares the converged hybrid solutions of pressure and x-velocity with the exact solution in the entire domain. The DSMC solution in the entire domain is considered as the exact solution and comparisons are made across two selected sections by plotting the velocities along two straight lines located at a height of $0.15H_1$ and $0.35H_1$ above the bottom wall. Comparison of pressure is made across just one section which is at a height of $0.15H_1$ above the bottom wall, since the variation of pressure is negligible along the thickness of the bearing. In the figure the vertical lines denote the overlap region. The solutions of both pressure and velocity show good correlation with the exact solutions with a maximum deviation of about 5% observed. The pressure in the region outside the slider remains about the ambient pressure, while that near the inflow and outflow of the slider deviates from the ambient pressure of 1 atm. At the inflow there is a significant increase in pressure, while at the outflow the pressure drops below the ambient pressure, which affects the pressure profile in the slider bearing region. From the solutions of velocity, it can be observed that the velocity values under the slider are characterized by slip and rises to a peak value at the trailing edge of the slider where there is a sudden pressure drop.

4.2.1. Effect of size of overlap region on convergence. The effect of size of the overlap region on the convergence of the hybrid Schwarz method is investigated by considering different overlap widths along the *y-overlap* region. The variation of computed velocity and pressure boundary conditions transferred from the continuum domain to the DSMC sub-domain with different overlap width size is shown in Figure 20. The boundary condition value along the *y-overlap* is plotted by taking the corresponding values of pressure and velocity from the buffer cell at $l_{\text{ext}}/2$. The error in the transferred boundary conditions of pressure and velocity from the continuum domain to

DOI: 10.1002/fld

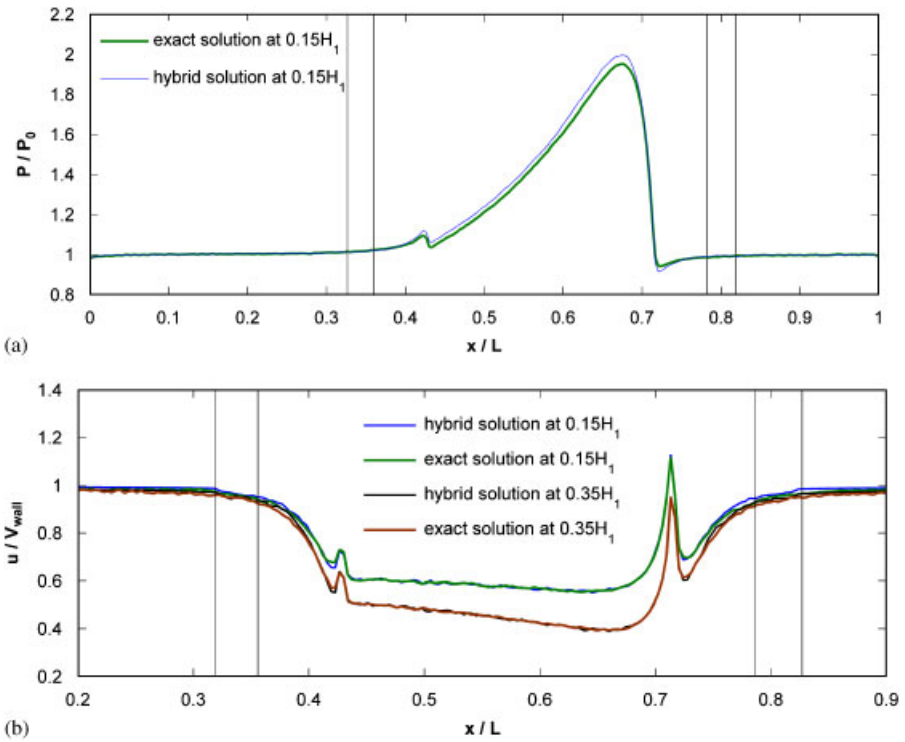

Figure 19. Comparison of hybrid solutions of: (a) pressure and (b) *x-velocity* with the exact solution in the entire domain.

the DSMC sub-domain along the *y-overlap* region is shown in Figure 21 by plotting the relative error norm with respect to the exact solution. For example, the relative error norm for pressure is calculated as $\sum\sqrt{(P_{\text{exact}}-P)^2/P_{\text{exact}}^2}$, where P_{exact} is the exact solution.

It is observed from Figures 20 and 21 that the Schwarz method for NS/DSMC coupling does not converge when the overlap is zero. Both the pressure and velocity values appear to diverge with Schwarz iterations in the absence of an overlap region. For all the other cases of overlap width considered viz; $w=26$, 39, 52 nm, the convergence is not significantly affected with variation in the overlap. With increasing overlap size, the convergence is only slightly improved, with no significant variations observed. The results indicate that the hybrid coupling by the Schwarz method is weakly dependent on the size of the overlap region. However, a finite overlap must be employed to facilitate the exchange of boundary conditions as the hybrid solution could diverge with zero overlap.

4.2.2. Comparison of continuum solutions with hybrid solutions. An investigation is done to study the impact of rarefied flow effects on flow prediction in the vicinity of the HDI region by comparing the computed flow field in the entire domain obtained using the NS equations with the hybrid continuum–atomistic solution in the entire domain. The comparisons of the continuum solutions of pressure and velocity with the hybrid solutions along the disk surface are plotted

DOI: 10.1002/fld

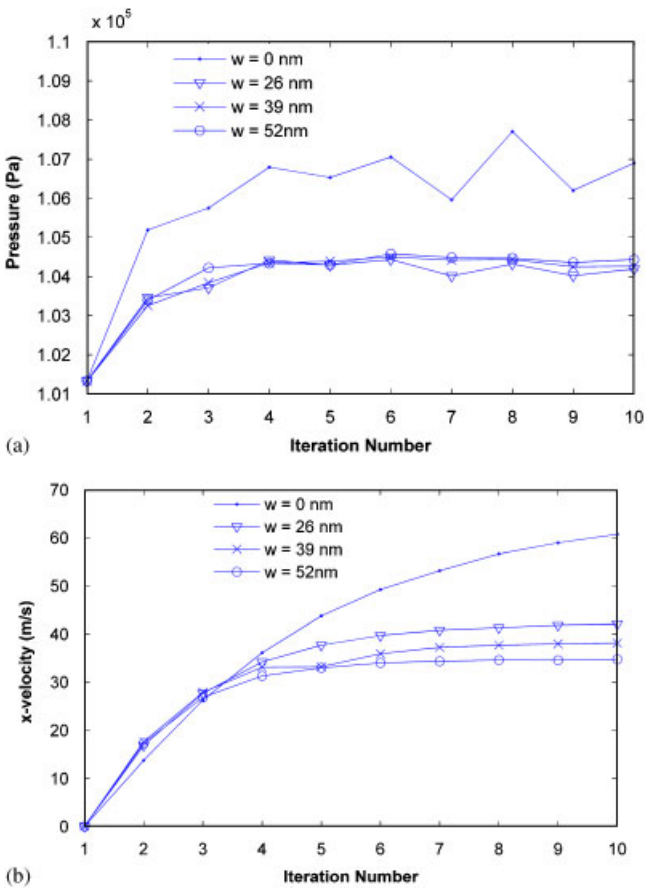

Figure 20. Convergence of: (a) pressure and (b) *x-velocity* component with Schwarz iterations as a function of overlap size.

in Figure 22. The region between the two vertical lines denotes the slider bearing region. The continuum solutions overpredict the solutions of both pressure and velocity. The peak pressure predicted by the continuum method varies by about 50% from the hybrid solutions. The flow in the slider falls in the transition regime and hence the continuum solutions cannot predict the rarefied flow effects like velocity slip as could be observed from the velocity plot comparison.

5. CONCLUSIONS

In this work, flow modeling for micro flow simulations using DSMC method is discussed in detail both for a stand-alone DSMC computations and a hybrid continuum–atomistic simulation in which a NS solution is coupled to a DSMC solution. An appropriate implicit boundary treatment method for modeling inflow and outflow flow simulation. An investigation into the number of cells required for an accurate DSMC simulation of the HDI gap reveals that the linear cell dimensions

DOI: 10.1002/fld

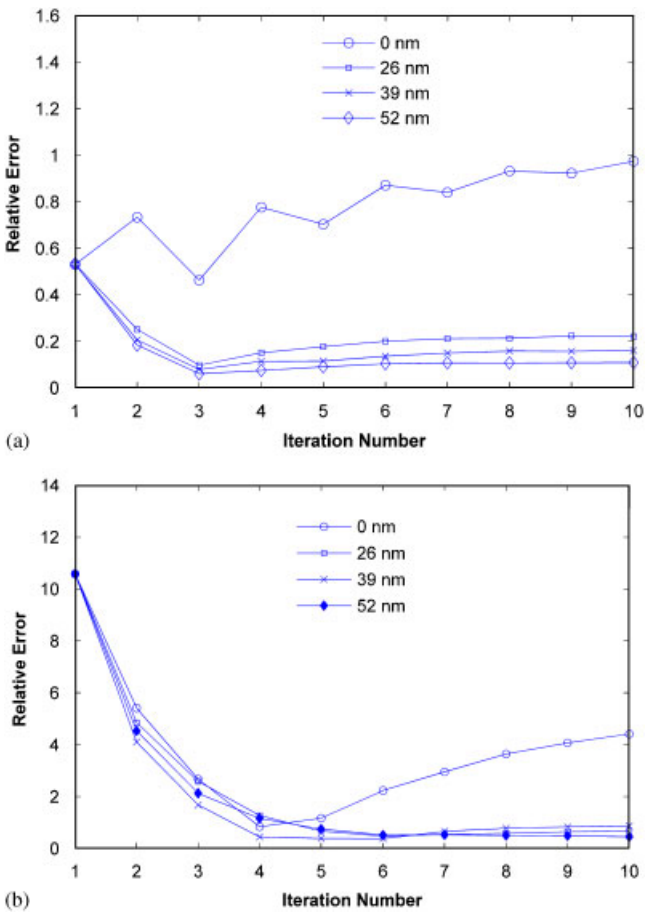

Figure 21. Convergence of relative error norm of: (a) pressure and (b) *x-velocity* component along the *y-overlap* boundary with Schwarz iterations as a function of overlap size.

along the length and width of the slider can be much greater than the mean-free path because of very small velocity gradients along these directions. This effectively reduces the total number of cells and particles required to ensure an accurate DSMC simulation of the HDI gap. A hybrid continuum–atomistic method for micro flows based on the Schwarz alternating method is applied to compute flow in the HDI gap. The hybrid coupling has been demonstrated in two dimensions by considering overlap regions along both the x and y directions. Boundary condition imposition from the continuum region to the DSMC region has been achieved with the aid of buffer cells and Chapman–Enskog velocity distribution. To reduce the computational cost associated with the DSMC method, the DSMC sub-domain has been parallelized. Converged hybrid flow solutions are obtained in about five iterations and the hybrid DSMC–NS solutions show good agreement with the exact solutions in the entire domain considered. A study on the impact of the size of the overlap region on the convergence behavior of the Schwarz method shows that a finite overlap region is essential for the convergence of the Schwarz method, as the hybrid solutions have been found to diverge when an overlap of zero width is considered. For all other cases of finite overlap

DOI: 10.1002/fld

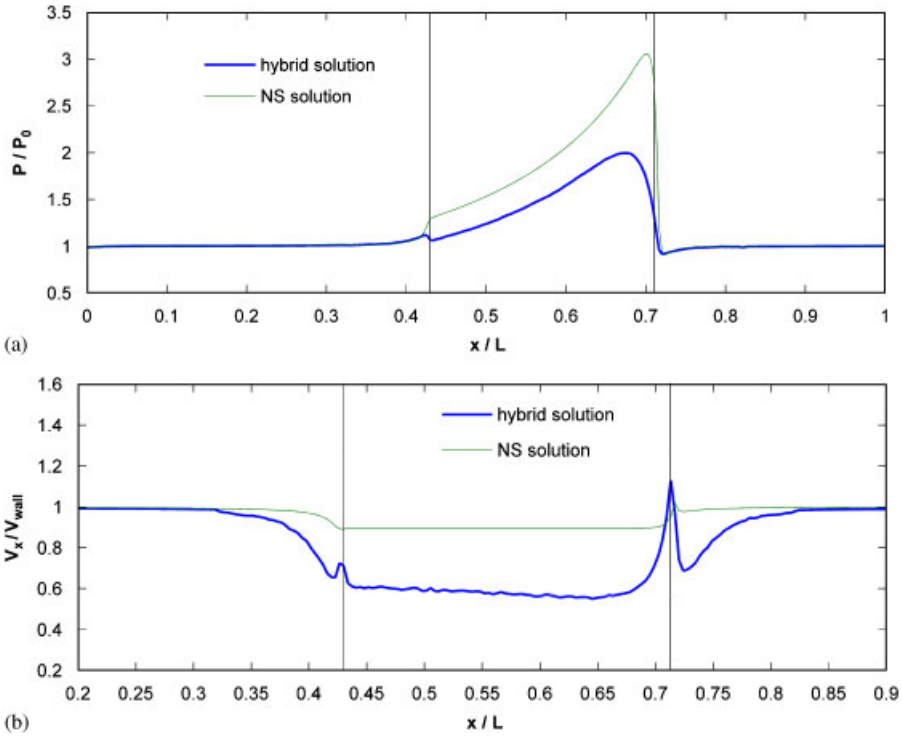

Figure 22. Comparison of Navier–Stokes (continuum) solutions of: (a) pressure and (b) *x-velocity* with the hybrid solutions in the entire domain.

sizes, no significant variations in the convergence behavior are noted. The impact of rarefied flow effects on the flow prediction in the vicinity of the HDI region has also been investigated by comparing the flow field obtained using the NS equations in the entire domain with the accurate hybrid solutions.

ACKNOWLEDGEMENTS

This work is part of a joint research project funded jointly by Seagate Technology International and Nanyang Technological University.

REFERENCES

1. Ali S, Damodaran M, Ng QY. Wall shape effects on airflow characteristics in hard disk drive enclosures. *Progress in Computational Fluid Dynamics* 2006; **6**(8):511–521.
2. Ali S, Damodaran M, Ng QY. Computational models for predicting airflow induced particle contamination in hard disk drive enclosures. *AIAA 17th Computational Fluid Dynamics Conference*, Toronto, Canada, *AIAA-2005-5342*, 2005.
3. Kubotera H, Tsuda N, Tatewaki M, Maruyama T. Aerodynamic vibration mechanism of HDD arms predicted by unsteady numerical simulations. *IEEE Transactions on Magnetics* 2002; **38**(5):2201–2203.
4. Shimizu H, Tokuyama M, Imai S, Nakamura S, Sakai K. Study of aerodynamic characteristics in hard disk drives by numerical simulation. *IEEE Transactions on Magnetics* 2001; **37**(2):831–836.

DOI: 10.1002/fld

5. Alexander FJ, Garcia AL, Alder BJ. Direct simulation Monte Carlo for thin-film bearings. *Physics of Fluids* 1994; **6**(12):3854–3860.
6. Huang W, Bogy DB, Garcia AL. Three-dimensional direct simulation Monte Carlo method for slider air bearings. *Physics of Fluids* 1997; **9**(6):1764–1769.
7. Bird GA. *Molecular Gas Dynamics and the Direct Simulation of Gas Flows*. Oxford: Clarendon, 1994.
8. Lilley CR, Macrossan MN. Methods for implementing the stream boundary condition in DSMC computations. *International Journal for Numerical Methods in Fluids* 2003; **42**(12):1363–1371.
9. Tysanner M, Garcia AL. Non-equilibrium behavior of equilibrium reservoirs in molecular simulations. *International Journal for Numerical Methods in Fluids* 2005; **48**(12):1337–1349.
10. Chapman S, Cowling TG. *The Mathematical Theory of Non-Uniform Gases*. Cambridge University Press: Cambridge, 1960.
11. Ikegawa M, Kobayashi J. Development of a rarified gas flow simulator using the direct simulation Monte Carlo method. *JSME International Journal* 1990; **30**:463–467.
12. Nance RP, Hash DB, Hassan HA. Role of boundary conditions in Monte Carlo simulation of MEMS devices. *Journal of Thermophysics and Heat Transfer* 1998; **12**(3):447–449.
13. Wu JS, Tseng KC. Analysis of micro-scale gas flows with pressure boundaries using direct simulation Monte Carlo method. *Computers and Fluids* 2001; **30**(6):711–735.
14. Fang Y, Liou W. Computations of the flow and heat transfer in microdevices using DSMC with implicit boundary conditions. *Journal of Heat Transfer* 2002; **124**(2):338–345.
15. Wang M, Li Z. Simulations for gas flows in micro geometries using the direct simulation Monte Carlo method. *International Journal of Heat and Fluid Flow* 2004; **25**(6):975–985.
16. Hadjiconstantinou NG. Discussion of recent developments in hybrid atomistic–continuum methods for multi-scale hydrodynamics. *Bulletin of the Polish Academy of Sciences*, *Technical Sciences* 2005; **53**(4):335–342.
17. Wijesinghe S, Hadjiconstantinou NG. Discussion of hybrid atomistic–continuum methods for multi-scale hydrodynamics. *International Journal for Multiscale Computational Engineering* 2004; **2**:189–202.
18. Garcia AL, Bell JB, Crutchfield WY, Alder BJ. Adaptive mesh and algorithm refinement using direct simulation Monte Carlo. *Journal of Computational Physics* 1999; **154**:134–155.
19. Hash DB, Hassan HA. Two-dimensional coupling issues of hybrid DSMC/Navier–Stokes solvers. *The 32nd AIAA Thermophysics Conference*, Atlanta, GA, *AIAA Paper 97-2507*, 1997.
20. Wadsworth DC, Erwin DA. Two-dimensional hybrid continuum/particle simulation approach for rarefied hypersonic flows. *AIAA Paper 92-2975*, 1992.
21. Schwartzentruber TE, Boyd ID. A hybrid particle–continuum method applied to shock waves. *Journal of Computational Physics* 2006; **215**:402–416.
22. Quarteroni A, Valli A. *Domain Decomposition Methods for Partial Differential Equations*. Oxford: Clarendon, 1999.
23. Hadjiconstantinou NG. Hybrid atomistic–continuum formulations and the moving contact-line problem. *Journal of Computational Physics* 1999; **154**:245–265.
24. Werder T, Walther JH, Koumoutsakos P. Hybrid atomistic–continuum method for the simulation of dense fluid flows. *Journal of Computational Physics* 2005; **205**:373–390.
25. Aktas O, Aluru NR, Ravaioli U. A combined continuum/DSMC technique for multi-scale analysis of microfluidic filters. *Journal of Computational Physics* 2002; **178**:342–372.
26. Memnonov VP. Coupling scheme for continuum and parallel DSMC parts to a numerical solution of a two-dimensional subsonic problem. *Parallel Computational Fluid Dynamics—Advanced Numerical Methods*, *Software and Applications* 2003; 89–96.
27. Benzi J, Damodaran M. Hybrid flow modeling in the head–disk interface region in small form factor hard disk drive enclosures. *Proceedings of the Seventh Asian Computational Fluid Dynamics Conference* (*ACFD7*), Bangalore, India, 26–30 November 2007.
28. Hadjiconstantinou NG, Garcia AL, Bazant MZ, He G. Statistical error in particle simulations of hydrodynamic phenomena. *Journal of Computational Physics* 2003; **187**:274–297.
29. FLUENT Inc. *Flow Simulation Software User Guide* (*Fluent 6.1.2*), 2003.
30. Garcia AL, Alder BJ. Generation of the Chapman Enskog distribution. *Journal of Computational Physics* 1998; **140**:66–70.
31. Benzi J, Damodaran M. Parallel three dimensional direct simulation Monte Carlo for micro flows. *Proceedings of the International Conference on Parallel Computational Fluid Dynamics* (*ParCFD' 07*), Antalya, Turkey, 21–24 May 2007.

DOI: 10.1002/fld